WIGGLER OPTIMIZATION FOR EMITTANCE CONTROL: EXPERIENCE AT CESR-C*

A. Temnykh† for CESR operating group,
Cornell University, Ithaca, NY 14850, U.S.A.

* Work supported by the US National Science Foundation
† E-mail address: abt6@cornell.edu

Abstract

To enhance radiation damping at J/Psi meson energy range at CESR, we use super-conducting wiggler magnets. This paper, addressing the goals of Mini-Workshop on Wiggler Optimization for Emittance Control hold in INFN Frascati in February 2005, describes our experience obtained in course of the design, production and operation of the magnets. Most of the presented data was published previously in [4] and [5].

INRODUCTION

In 2001 the decision was made to modify the Cornell Electron Storage Ring **(**CESR**)** to provide luminosity over an energy range from 1.5 to 2.5GeV per beam. Previously CESR was operated at 5 GeV per beam energy with maximum luminosity $1.7\text{x}10^{33}$ $1/\text{cm}^2/\text{sec}$. The transition to lower energy reduces beam stiffness, radiation dumping and horizontal beam emittance. According to empirical law, luminosity scales with energy as $E^{-\alpha}$, where α is in range between 4 and 7, [1]. This scaling predicts luminosity at 1.8GeV from $2.2\text{x}10^{31}$ to $8.2\text{x}10^{28}$ $1/\text{cm}^2/\text{sec}$. Installation of the wiggler magnets can significantly enhance radiation damping and help to keep horizontal beam emittance constant. Under this condition luminosity will scale with energy as E^{-2}, which gives a peak luminosity ~$2\text{x}10^{32}$ $1/\text{cm}^2/\text{sec}$. The enhanced radiation damping increases injection rate and improved beam stability. Herein lies the importance of the wiggler magnets for CESR-c project.

WIGGLER MAGNET MAIN PARAMETERS SETTING

Peak field, total length and period

In a storage ring with radiation dominated by wiggler magnets, the following scaling can be applied to radiation damping time τ, horizontal beam emittance ε_x and beam energy spread σ_E:

$$\frac{\sigma_E}{E_0} \propto \sqrt{B_w} \quad (1)$$

$$\tau \propto \frac{1}{B_w L_w} \quad (2)$$

$$\varepsilon_x \propto B_w H_w \quad (3)$$

Here, B_w is the wiggler peak field, L_w is the total length of the wiggler magnets and H_w is dependent on optic functions. If beam parameters are chosen, these equations impose constrains on wigglers. For instance, Equation (1) points that wiggler peak field B_w will be limited by maximum allowable beam energy spread. In the case of CESR-c, maximum allowable beam energy spread $0.8\text{x}10^{-4}$ limits peak field to 2.1T. The maximum energy spread was determined from horizontal beam size limit in arcs. According to equation (2), to provide reasonable radiation damping time, ~50ms, comparable with damping at 5GeV, the wiggler active length should be ~20m. Horizontal beam emittance can be controlled by H_w, see equation (3).

The wiggler period, λ, was chosen from the following consideration. According to references [2] and [3] particles entering the wiggler with vertical and horizontal coordinates y and x will be deflected at the end of wiggler by angles dy' and dx':

$$dy' = -\frac{B_w^2 L}{2(B\rho)^2}\left[y + \frac{2}{3}\left(\frac{2\pi}{\lambda}\right)^2 y^3 + \ldots \right] \quad (4)$$

$$dx' = -\frac{B_w L}{2(B\rho)^2}\frac{\partial B_y(x)}{\partial x}\left(\frac{\lambda}{2\pi}\right)^2 \quad (5)$$

Where $B\rho$ is beam stiffness, $B_y(x)$ describes dependence of vertical magnetic field on horizontal position across the wiggler pole. In the vertical plane, the first term in equation (4) $\propto y$ gives a linear focusing effect, the second octupole-like term $\propto y^3$ results in vertical nonlinear focusing. The letter causes dependence of vertical betatron tune on vertical amplitude, vertical orbit position, and may drive nonlinear resonances. Note that this term $\propto \lambda^{-2}$, i.e, it is smaller for longer period. Nonlinearity in the horizontal plane, see equation (5), is due to variation of vertical field across the wiggler pole and $\propto \lambda^2$. In contrast to vertical, it is smaller for shorter wiggler period.

The above consideration provides guidance for a wiggler optimization strategy. First, one should minimize field variation across the pole by optimizing gap-to-width ratio and pole profile, then choose period based on a compromise between vertical and horizontal nonlinearity.

The first version of the CESRc wiggler model had 20 cm wide flat poles and 76.2mm gap and 20cm period. The gap size was chosen to accommodate a 50mm high beam pipe and the pole width was maximized to a reasonable limit. Tracking through the CESR magnetic structure with this type of wigglers indicated the storage ring dynamic aperture limitation in both planes due to wigglers nonlinearity. When we optimized wiggler pole profile to minimize $B_y(x)$ variation and increased wiggler period to 40cm, nonlinearities in both planes were significantly reduced and dynamic aperture became satisfactory.

Technology choice

It was clear from the beginning that the wiggler structure should be modular. Various technical considerations led us to chose the module length of ~1.5m with wiggler active length ~1.3m. To provide the needed 20m of total active magnetic length, 15 such modules should be inserted in the ring magnetic structure. Available space reduced this number to 12. The following options were considered for technology:

- Normal conducting copper/iron magnets. Based on existing magnets, we estimated that each module would require ~300kW of power. Because of limited space, it was problematic to fit adequate power supplies and cooling lines into tunnel.
- Permanent magnet (NbFeB). The required 2.1T field is higher than the typical field for PM magnets ~1.4T or less. To provide 2.1T field level in 50mm gap, magnetic design should be rather complicated and will require a large mass of expensive permanent magnetic material. An additional complication arises from fact that ~50% of time CESR should run at high energy, 5GeV per beam, as a synchrotron light source. During these periods of operation the PM wiggler magnets should either be removed from the ring or their poles opened. Neither option is practical.
- Superferric technology (iron poles and superconducting coils) seemed to us to be the only viable option for required 2.1T field over the given beam aperture. In this type of magnet we can easily control the magnetic field using small, ~1kW, power supplies. The power supplies can be located nearby magnets and cryogenic lines can be also easily fitted in tunnel.

Taking into account arguments listed above we made the choice in favor of superferric magnets.

Symmetric versus asymmetric magnetic design

We explored two types of the magnetic design: symmetric, 7 pole, and asymmetric, 8 pole. A schematic view of 7 pole version is shown in Fig. 1. The 8 pole version is very similar. Field distribution and beam trajectory along the magnets for both are depicted in Fig. 2 and **3**.

In the symmetric design there are two types of poles: "full strength" 20cm long and "1/2 strength" 15cm long. Five 20cm poles are located in the middle and two 15 cm poles at the ends. The resulting field is symmetric relative to the middle point. The trajectory lies on one side from the wiggler center and has 3.6mm of maximum excursion. For 2.1T of peak field integral $\int B_y^2(z)dz = 2.5\mathrm{T}^2\mathrm{m}$. The Octupole like moment in vertical plane $b_3 = -1.98\times10^4\mathrm{m}^{-3}$.‡

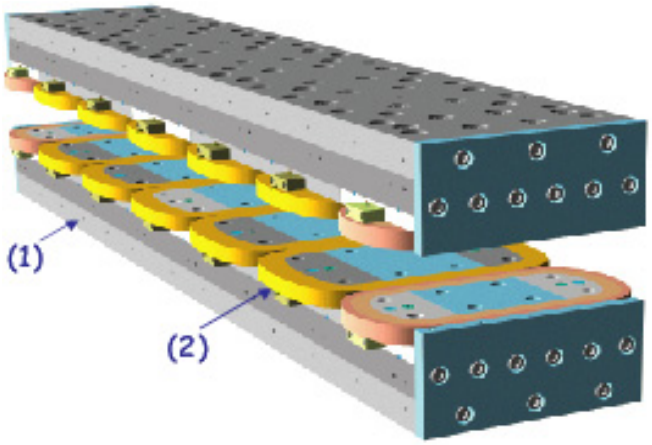

Figure 1: Schematic view of 7 pole wiggler. Here (1) is yoke plate of 7cm thick, 20cm wide and 130cm long used for flux return and poles support, (2) is pole pieces with super-conducting coil. Gap between halves is 7.62cm

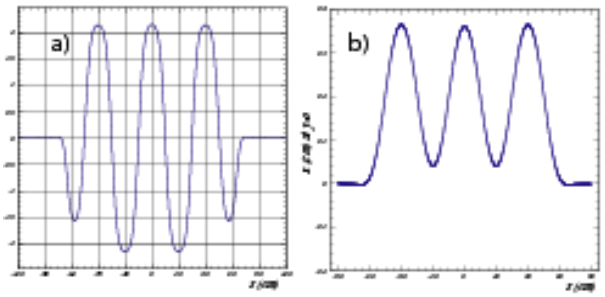

Figure 2: Symmetric (7pole) design. Plot (a) is the calculated vertical field and plot (b) the trajectory along the magnet. Vertical scale is 0.5T/division for (a) and 1mm/division for (b). Horizontal scale 10cm/division for both.

‡ We use definition $dy' = \sum_n b_n y^n$

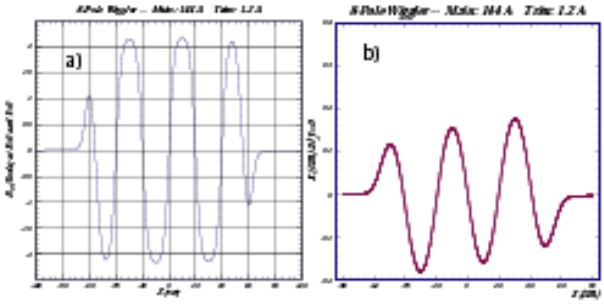

Figure 3: Asymmetric (8pole) design. Plot (a) is calculated vertical field and plot (b) trajectory along the magnet. Vertical scale is 0.5T/division for (a) and 1mm/division for (b). Horizontal scale 10cm/division for both.

The asymmetric design (8 pole), figure 3, has three types of poles, two 10cm long ("1/4 strength") at the ends, then two 15cm ("3/4 strength") and four 20cm ("full strength") poles in the middle. The field is asymmetric relative middle point. The trajectory is almost symmetric relative to the wiggler center with 1.8mm of maximum excursion. $\int B_y^2(z)dz$ =2.5T^{2}m, b_3 = -2.08x10^{4}m^{-3} are very close to those in the symmetric design.

Although both designs look very similar, asymmetric has specific features. First, because of asymmetry, any systematic errors in poles cancel each other, i.e., field integrals depend only on random errors and are not sensitive to systematic. This characteristic significantly facilitates production and quality control. Another feature is in the dependence of field integrals on excitation. Any field distortions due to iron saturation will cancel each other in asymmetric design, but in symmetric will not. Magnetic measurements described in the following section confirm this.

It should be mentioned that the choice between symmetric and asymmetric design was not obvious. First, we built prototype with symmetric field, but after magnetic field measurement and characterization with beam in machine, we made decision in favor of asymmetric design.

SUPER-CONDUCTING COILS PRODUCTION CONTROL

The program for production and testing of CESR-c wiggler magnets was outlined in reference [5]. Here, we focus on some details critical to field quality, which were mentioned but not elaborated in this reference.

The wiggler overall performance and reliability depend critically on the quality of the pole pieces. The missing or extra turns in super-conducting coils can result in unacceptable magnetic field distortion. Turn-to-turn shorts may cause magnet destruction during quench. In addition, errors in the coil transfer dimensions may produce significant skew-quadrupole component in wiggler field. To control the pole pieces quality we employed two types of warm magnetic measurements. The first is to detect missing, extra or shorted turns and the second to test coils transfer dimension.

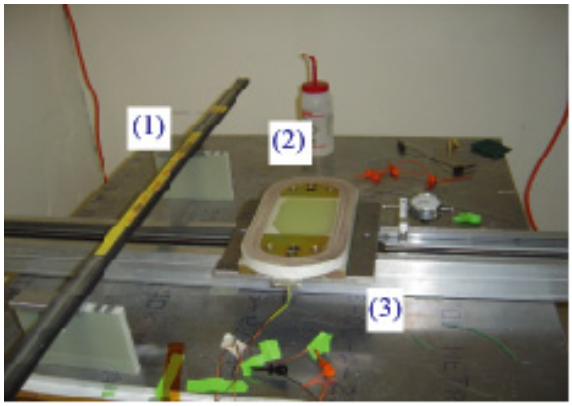

Figure 5: Warm magnetic measurement setup for missing turns test. (1) is 1.2m long, 1cm wide pickup coil consisted of 2000 turns: (2) is tested pole: (3) is sliding stage.

The setup for missing or shorted turns detection is depicted in Fig. 5. It consisted of a pickup coil, integrating voltmeter and sliding stage controlled by a stepping motor. In process of measurement the tested pole piece, mounted on sliding stage and energized by 1A of DC current, was moved step by step under the pickup coil. The voltage induced in the pick up coil by the pole magnetic field was measured and integrated by voltmeter. For this type of measurement the pole orientation was such that it was moving parallel to beam axis. In this way we measured the field profile in "z" direction. One thoroughly checked pole was chosen to be a standard and its field profile was used as a reference. By analyzing deviation of the tested pole field from reference one can easily detect problems. Missing or shorted turns result in weaker field. Extra turns make field stronger.

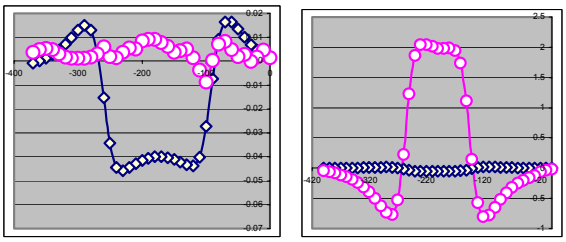

Figure 6: Tested pole field profile in "z" direction (diamonds) and it's deviation from reference (circles) multiplied by a factor 660. Horizontal scale is in mm, vertical in relative units. Left plot illustrates sensitivity of the method, right plot is the test result of pole with shorted coil (pole F105, tested 12/16/02). Note the right plot has vertical scale 14 times larger than the left.

Plots in Fig. 6 present the tested pole field profiles and its deviation from reference. The left plot illustrates resolution. Here, we used the "standard" pole in the test. The deviation of the measured field ratio is ~$4x10^{-4.}$ This is the method resolution. Right plot presents result of one of 15cm poles testing, (F105, test on 12/16/05). A large, ~6%, field difference from reference indicated the shorted coil. This pole was later reworked.

All of ~260 poles built for wigglers were measured before assembly and compared with "standard" poles. Approximately 10 of them were found to have problems with coils and were rewound.

In the course of wiggler magnet production we found that errors in the coil transfer dimensions may result in significant skew-quadrupole component in assembled wigglers. Fig.7 shows the picture of a single pole with marked coil regions where dimensions are critical for skew-quad component. On left side is given an explanation of the mechanism of the skew component generation.

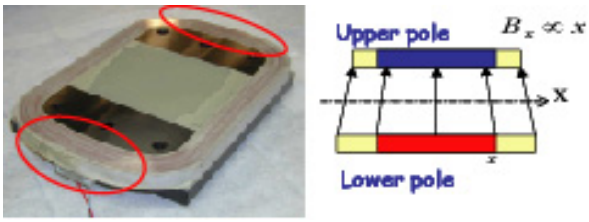

Figure 7. Pole piece with marked super-conducting coil region with critical dimension. On right side an explanation of how errors in coil dimension result in skew-quad component.

To test transverse coil dimensions we used the same setup, see Fig. 5, but the tested pole orientation was different. It was rotated by 90 degrees. In this way we measured the field profile in "x" direction. One example of this measurement is presented on Fig. 8.

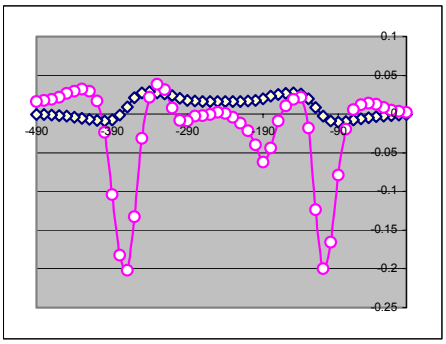

Figure 8: Tested pole field profile in "x" direction (diamonds) with deviation from reference (circles). Horizontal scale is in mm, vertical scale in relative units. Deviation is multiplied by a factor 660.

One can see two peaks in deviation located at the ends of the pole. Knowing the horizontal scale, the slope in dependence of field on "x" and the peak amplitudes one can estimate the difference in coil dimension from the "standard" pole. In this particular case the tested pole was 0.4mm narrower than the "standard". Note that this difference in dimension was due to the super-conducting coil, not due to the iron. Having information about poles' (coils) dimension we optimized the poles distribution in wigglers to minimize integrated skew-quadrupole component.

MAGNETIC FIELD MEASUREMENT

For magnetic field measurement we used traditional Hall probe mapping and flipping coil techniques.

The result of magnetic field measurement with Hall probe of 7 pole wiggler (unit#1) at 2.1T of peak field is shown in Fig. 9. Here, the left plot presents measured and calculated vertical magnetic fields along magnet, the right plot shows the difference between them. On the left plot one can see rather remarkable agreement between calculation and measurement.

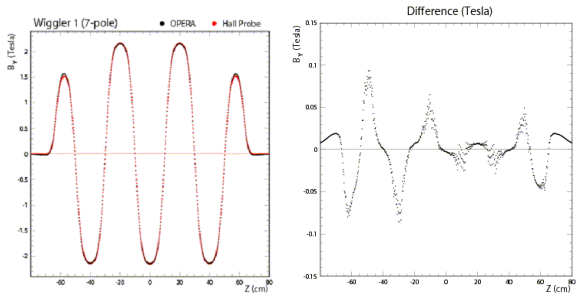

Figure 9: Hall probe measurement. Left plot shows vertical the field along a 7 pole wiggler measured with Hall probe and calculated field. Right plot is the difference between measured and calculated field. Horizontal scale is 20cm per division, vertical scale 0.5T per division on left plot and 0.05T per division on right.

However, the right plot indicates the difference with maximum ~100G and, what is more important, the data spread in locations with high gradient at level of 20G. The spread suggests that while Hall probe measurement is satisfactory for general purposes, it is insufficient for precise field integral measurements. For these purposes we used a long flipping coil setup described in reference [6]. Figures 10 and 11 present the flipping coil measured dependence of vertical field integral versus horizontal position for various excitation levels. Figure 10 depicts the measurement for a symmetric (7pole) wiggler, unit #1, and Figure 11 shows the result for asymmetric (8pole) wiggler, unit #4.

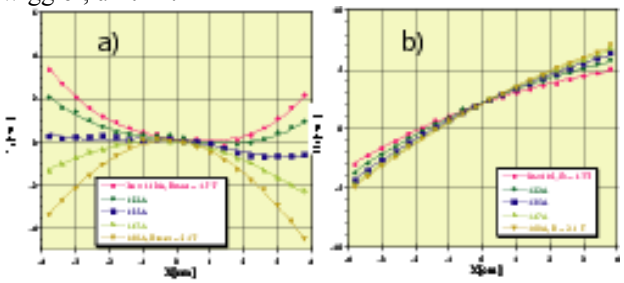

Figure 10: Symmetric (7pole) wiggler magnetic measurement. Vertical (a) and horizontal (b) magnetic field integrals versus horizontal position for peak field in range from 1.7 T (circles) to 2.1 T (triangles). Vertical scale is 2 Gm/division for a) and 5 Gm/division for b), horizontal 1 cm/division.

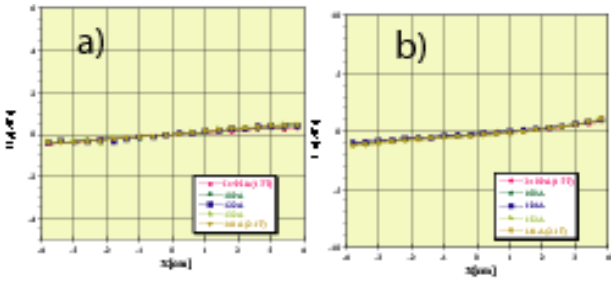

Figure 11. Asymmetric (8 pole) wiggler magnetic measurement. Vertical (a) and horizontal (b) magnetic field integrals versus horizontal position for peak field in range from 1.7 T (circles) to 2.1 T (triangles). Vertical scale is 2 Gm/division for a) and 5 Gm/division for b), horizontal 1 cm/division.

Comparing vertical field integrals for different excitation levels, Figures 10 and 11, in symmetric and asymmetric design one can see that asymmetric (8 pole) wiggler maintains linearity over wider range.

Skew-quadrupole moment, seen as a variation in horizontal field integral with horizontal position, was point of the great concern because coupling between horizontal and vertical motion may result in growing vertical beam emittance. As mentioned in previous section, we found that this moment was caused by errors in the transverse dimension of super-conduction coils.

The magnetic field of all 14 wigglers we built was measured with a Hall probe and long flipping coil. Results of the measurements were taken into account in the selection of the location of wigglers around ring.

RESOURCES AND COST

During the production cycle the following resources were committed to the project:

- Senior technical and supervisory staff: 5 full time employs
- Technical supporting staff: 13 full time employs

Approximate cost per wiggler unit for parts and outside machining and manufacturing ~ $80k.

Production rate was one wiggler every 3 weeks.

BEAM PARAMETERS AND BEAM BASED WIGGLER CHARACTERIZATION

In this section we compare measured and calculated CESR-c beam parameters critically dependent on wiggler field and report results of beam based wiggler field characterization.

Model

The ring model we use in calculation of beam properties is based on the BMAD subroutine library developed by D. Sagan [7]. The model incorporates calculated 3D wiggler magnetic field map [8].

Bunch length and beam energy spread: measurement and model prediction

Figure 12 illustrates a bunch length measurement with streak camera for CESR-c optics "12WIG_20050208" with 2.1 T peak field in the wigglers and ~9 MV of total accelerating RF voltage.

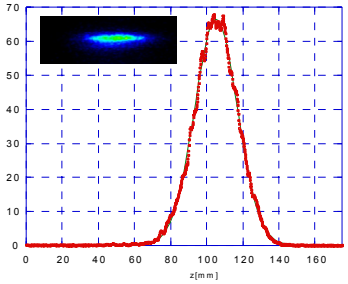

Figure 12: Longitudinal particle density distribution in bunch measured with streak camera.

Plot shows the longitudinal particle density distribution in a single bunch. Fitting with a Gaussian gave a bunch length $\sigma_z = 11.86 \pm 0.03 mm$. Beam energy spread can be calculated from the expression:

$$\frac{\sigma_E}{E} = \frac{2\pi f_S}{c|\eta|}\sigma_z \quad (6)$$

Where c is speed of light, η-momentum compaction factor, f_s- synchrotron tune, see reference [9]. For CESR-c parameters f_s = 39kHz and η = 0.011 it gives $\frac{\sigma_E}{E} = 8.62 \times 10^{-4}$ which is very close to predicted 8.47×10^{-4}. It should be mentioned that the radiation in wiggler magnets absolutely dominates over radiation in the rest of the ring. Thus, the fact of good agreement between measured and calculated spread, the spread being formed by radiation, means good agreement between model and reality.

Beam based wiggler field characterization.

To characterize the wiggler field two types of experiments were carried out. The first was the measurement of betatron tune variation with wiggler current. Another was the measurement of betatron tunes as a function of beam position in wigglers and as a function of betatron amplitude.

The tune variation with wiggler current is the consequence of a linear focusing effect of the wiggler field. Expressions for tune variation with current derived from equations (4) and (5) are:

$$\Delta Q_y = \frac{\beta_y}{4\pi}\frac{B_w L}{(B\rho)^2}\frac{dB_w}{dI}\Delta I \quad (7)$$

$$\Delta Q_x = \frac{\beta_x}{4\pi}\frac{L}{(B\rho)^2}\frac{\partial^2 B_y}{\partial x^2}\left(\frac{\lambda}{2\pi}\right)^2\frac{dB_w}{dI}\Delta I \quad (8)$$

In the experiment we changed the current of one of the wigglers (14WA) in a range from 141 A to 138 A and measured vertical and horizontal betatron tunes. Figure 13 presents the result. Here are measured and calculated tune variation as a function of current. For calculation we used expressions (7) and (8) with parameters $\frac{\partial^2 B_y}{\partial x^2}$ and $\frac{dB_w}{dI}$ from a 3D magnetic field calculation.

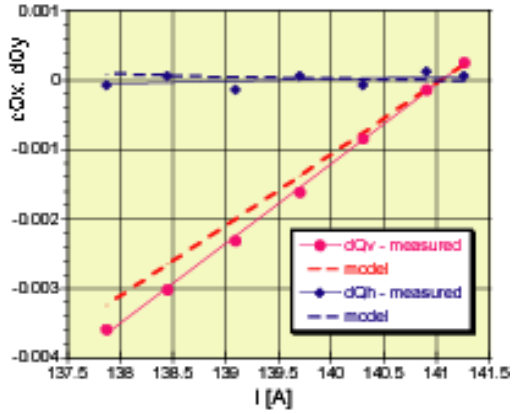

Figure 13: Betatron tune as a function of wiggler 14AW current. Circle and diamonds are for vertical and horizontal tunes. Dashed lines show calculated dependence.

A linear fit of the measured dependence of vertical tune on current gives $\Delta Q_y / \Delta I = 1.15 \times 10^{-3}$ 1/A. That is very close to model prediction, 1.02×10^{-3} 1/. The very weak dependence of horizontal tune on current predicted in

model, $\Delta Q_x / \Delta I = -3.0 \times 10^{-5}$, was also confirmed in experiment, $(3.0 \pm 2.5) \times 10^{-5}$ 1/A.

Measurement of betatron tune as function of vertical and horizontal beam position was the second type of experiment. The measured and calculated dependence of betatron tune on vertical and horizontal beam position in wigglers are given in Figures 14 and 15. In this experiment we tested a group of 3 wiggler magnets at 18E location. For vertical and horizontal beam orbit displacement we used localized orbit distortions called "closed bumps". All nonlinear magnetic elements, mostly sextupole magnets, in the closed bumps region during measurements were turned off.

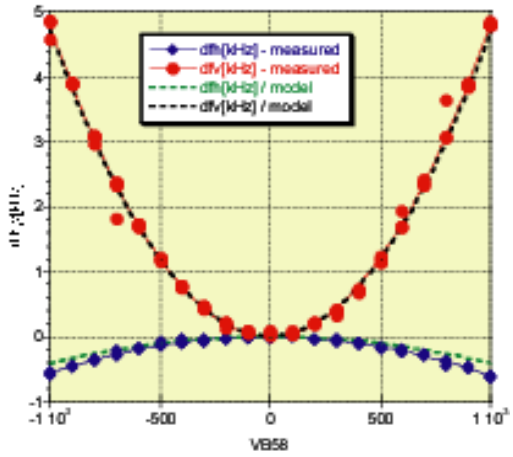

Figure 14: Vertical (circles) and horizontal (diamonds) betatron tune variation versus vertical beam position in 18E wiggler cluster (group of 3 wigglers). Modeled dependence is given by dashed line. Vertical scale is 1kHz or 0.0025 per division, horizontal ~ 5mm per division.

Figure 14 shows a large quadratic variation of vertical tune with vertical beam position and much smaller variation of horizontal tune. Both are in good agreement with calculation. Strong dependence of vertical tune on vertical position is a well known effect. It is due to interference between beam trajectory wiggling in horizontal plane and longitudinal magnetic field component seen by particles displaced vertically from the wiggler center.

Tune variation with horizontal position, see Figure 15, is smaller. This variation is caused by non-uniformity of magnetic field across wiggler poles. Here, one can see also a good agreement between measurement and calculation.

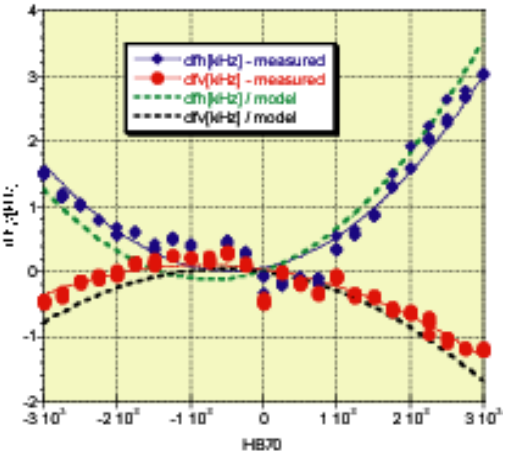

Figure 15: Vertical (circles) and horizontal (diamonds) betatron tune variation with horizontal beam position in 18E wiggler cluster (group of 3 wigglers). Modeled dependence is given by dashed line. Vertical scale is 1kHz or ΔQ= 0.0025 per division, horizontal ~ 5mm per division.

Data collected from testing of other wiggler magnets also showed good agreement with model predictions

CONCLUSION

- For CESR-c project we designed, built and tested 16 superferric wiggler magnets. 12 of them have been installed in the ring and now under operation.
- We found that beam parameters formed by wiggler magnets as well as beam based wiggler field characterization are in good agreement with model prediction. It means that we have a) good magnets, b) reliable model.
- So far we have not seen any beam performance degradation due to wiggler field nonlinearities.

We believe that experience obtained in the course of design, testing and operating of CESR-c wiggler magnets will be extremely useful in coming projects.

ACKNOWLEDGMENT

We would like to express our appreciation to technical supporting group and especially to William Trask and John Stilwell who wound most of 260 super-conducting coils for their steady and very thoughtful work.

REFERENCES

[1] D. Rice, Private communication.
[2] J.Corbett, Y. Nosochkov, Proc. 1999 PAC, p. 2358
[3] J. Safranek et al., Proc. EPAC 2000, p. 295
[4] D. Rice et al., " CESRC-c A Frontier Machine For QCD and Weak Decay Physics in The Charm Region," EPAC 2002, p. 428
[5] D. Rice et al.," PRODUCTION AND TESTING CONSIDERATIONS FOR CESR-C WIGGLER MAGNETS," PAC 2003, p. 167
[6] A. Temnykh, "Vibrating Wire and Flipping Coil Magnetic Measurement of a CESR-c 7-Pole Wiggler Magnet" PAC 2003, p.1026

[7] D. Sagan, http://www.lns.cornell.edu/~dcs/bmad

[8] D.Sagan et al., "ICFA Beam Dynamics Newletters 31, 2003" p.48

[9] A. Chao and M. Tigner, "Handbook of Accelerator Physics and Engineering", p. 187